Potassium Ion-Intervened Copper-Nickel Bimetallic Organic Framework with Potassium Hydrogen Phthalate Ligand for High-Performance Potassium Ion Hybrid Supercapacitors

Table 1. Comparative performance characteristics of CuNi-MOF with reported literatures.

Electrode materials	**Specific capacitance**	**Energy density**	**Power density**	**Ref**
CuCN-MOF	508 C g^{-1}at 1 A g^{-1}	68.175 Wh kg^{-1}	5.54 kW kg^{-1}	[1]
Ni-MOF	804 F g^{-1} at 1 A g^{-1}	31.5 Wh kg^{-1}	800 W kg^{-1}	[2]
Cu-PTA MOF	260.5C g^{-1} at 0.7 A g^{-1}	35.9 Wh kg^{-1}	5950 W kg^{-1}	[3]
Zn-doped Ni-MOF	1620F g^{-1} at 0.25A g^{-1}	-	-	[4]
NiCo-MOF	1700.40F g^{-1} at 0.5 A g^{-1}	-	-	[5]
NiCo-MOF	1303F g^{-1} at 1A g^{-1}	-	-	[6]
NiCo-MOF	1202F g^{-1} at 1A g^{-1}	49.4 Wh kg^{-1}	562.5 W kg^{-1}	[7]
Ni//Cu MOF	1,424 F g^{-1} at 2 A g^{-1}	57 Wh kg^{-1}	48,000 W kg^{-1}	[8]

Table 2. Comparison of the diffusion coefficient of potassium ions with other electrode materials.

Electrode Materials	Ion Diffusion Coefficient(cm^2/s)	Electrolyte	Methods	Ref
CuNi-KHP	1.48974×10^{-11}	6M KOH	CV	-
HKUST-1	5.8×10^{-10}	1M LiOH	EIS	[9]
MIL-53(Cr)	3.7×10^{-11}	NaPSS	EIS	[10]
NiP2@MHNC	1.1×10^{-10}	Na^+	EIS	[11]
NiCo-MOF@CoOOH@V_2O_5	10^{-11}-10^{-13}	Na^+	EIS	[12]
Ni-MOF	5.8×10^{-10}	1M NaOH	EIS	[13]
$Ni_3(HITP)_2$	8.5×10^{-11}	EMIM-BF_4	MD	[14]

Confirmation process of the amount of active substances in two electrodes of hybrid supercapacitor:

$$\frac{m^+}{m^-}=\frac{C^-\times\Delta V^-}{C^+\times\Delta V^+}$$

First, we calculated the amount of active material to be 3 mg by weighing the cathode electrode sheet. Then, the capacitance of commercial activated carbon was measured to be 150F g^{-1}, according to the formula above, we deduced that the specific mass required for the commercial activated carbon electrode was 6.3mg.

Table 3. The chemical components of the as-prepared samples confirmed by ICP-OES.

Samples	ICP-OES(wt%)

	C	O	Cu	Ni	K
CuNi-KHP	67.23	27.82	7.6	9.3	4.78

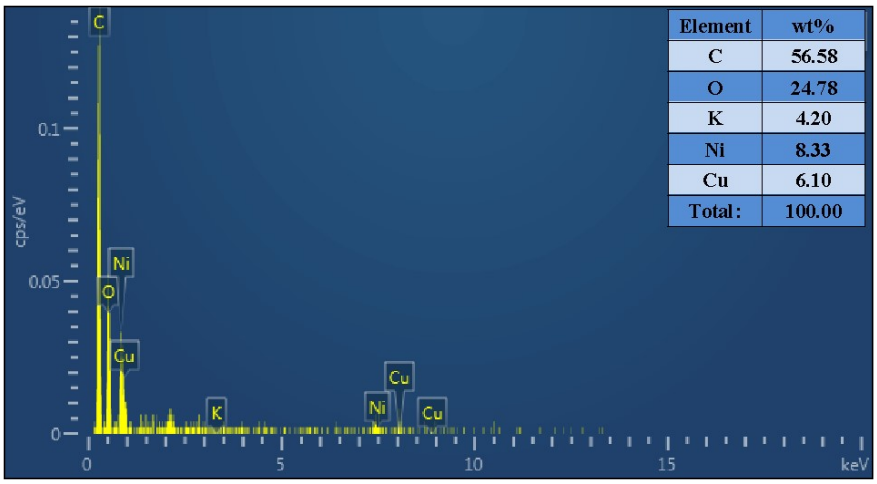

Fig S1. EDS elemental content distribution map

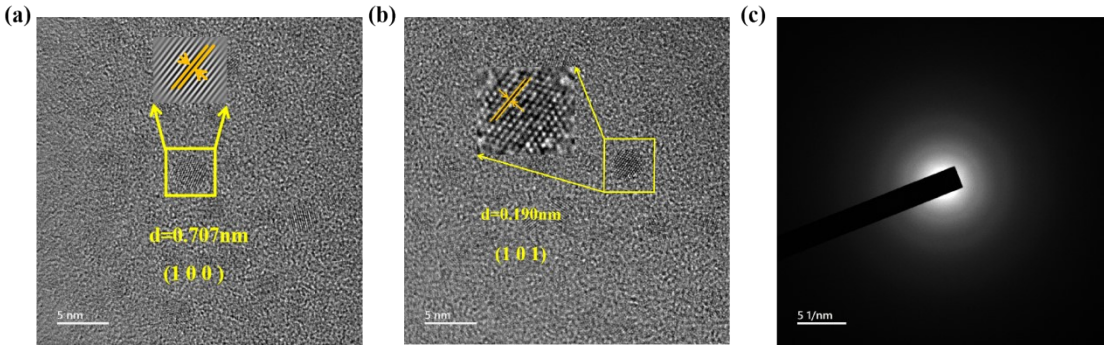

Fig S2. (a) (b)HRTEM image and (c) SAED pattern

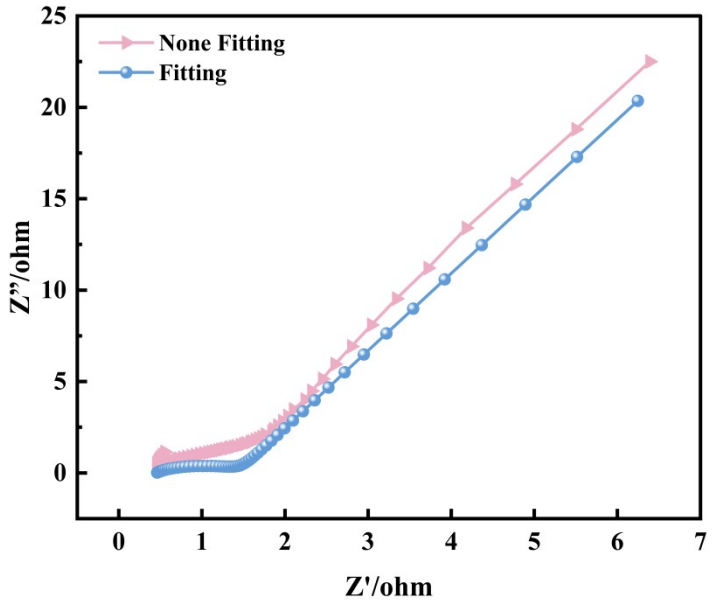

Fig S3. The Zview fitting comparison diagram

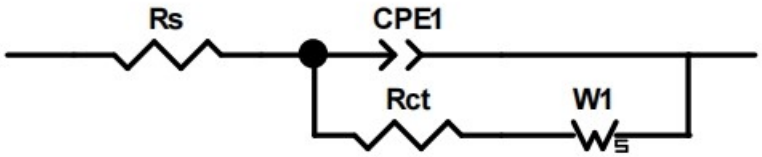

Fig S4. Equivalent circuit diagram

Mathematical Models for Electrochemical Kinetics

$$C_m(F/g) = \frac{\int IdV}{m \times v \times \Delta V} \quad \text{I}$$

$$Q(C/g) = \frac{I\Delta t}{m} \quad \text{II}$$

$$E(\frac{Wh}{kg}) = \frac{0.5 \times C\Delta V^2}{3.6} \quad III$$

$$P(\frac{W}{kg}) = \frac{3600 \times E}{\Delta t} \quad IV$$

where Cp is the specific capacitance F g^{-1}, Q is the specific capacity C g^{-1}, I / m is the applied current density A g^{-1}, $^{\Delta}$V is the applied potential V, E and P are the energy and power density, $\int IdV$ is the area of the closed curve of the CV diagram, m is the mass of the active substance, v is the scanning rate, and t is the discharge time.

To understand the charge-storage mechanism, we employed the the Power law method. According to this rule, the peak current response in the cyclic voltammetry (CV) is related to the scan rate (**v**):

$$i = va^b \quad V$$

$$\log i(v) = \log a + \text{b} \log v \quad VI$$

$$\text{i} = i_{cap} + i_{diff} = k_1 v + k_2 v^{0.5} \quad VII$$

$$\frac{\text{i}}{v^{0.5}} = k_1 v^{0.5} + k_2 \quad VIII$$

where a and b are constants for a system[15], i is the peak current in the CV plot and v is the scan rate.When the b-values are 0.5 and 1.0, they respectively indicate diffusion and capacitance control behavior. If the approximate value of b is close to 1, it indicates that the extrapolated pseudocapacitive electrode material is similar to a capacitive material, as they are primarily unaffected by diffusion. Calculated by formulas (*V*) and (*VI*), the b-values of the cathode and

anode of CuNi MOF are 0.2 and 0.35, respectively. This indicates that the electrode material primarily exhibits battery-like properties in the selected electrolyteas[16] shown in Figure 7a. Generally, the smaller the b-value, the greater the contribution of the diffusion-controlled insertion process, while the capacitance contribution increases with increasing b-value[17, 18].

The ion binding energy was calculated using density functional theory (DFT) with the DMo1 module in MaterialsStudio. Molecular geometry optimization was performed using the generalized gradient approximation (GGA) and Perdew-Burke-Ermzerhof (PBE) functional, ensuring that the maximum force did not exceed 0.002 Ha/Å and the maximum atomic displacement was less than 5×10^{-3} to guarantee convergence of the optimization results. The self-consistent field (SCF) convergence criterion was set below 10^{-5} eV to ensure the accuracy of electronic structure calculations. The binding energy (E) between potassium ions and the electrode material was calculated using the following formula:

To further verify the reaction mechanisms, we calculated the K-ion embedding energy for CuNi-KHP materials. The ion doping energies (E_{doping}) of can be calculated as follows:

$$E_{\text{doping}} = E_{*\text{k}} - E_k - E_{sub} \quad IX$$

Where E_K and E_{*K} represent the energies before and after the insertion of K^+ on the substrate, respectively, and E_{sub} is the energy of the pristine material surface. According to the above formula, the embedding energy ($E_{embedding}$) of K^+ on CuNi-KHP is -2.4 eV. This indicates a low energy barrier for ion embedding, making the electrode material more susceptible to the adsorption of K^+ from the electrolyte, thereby enhancing the specific capacity.

$$D_K = \left(\frac{I_P}{2.69\times10^5 \,\text{n}^{3/2} A C_0 v^{1/2}}\right)^2 \quad X$$

Furthermore, to gain a deeper understanding of the binding mechanism of potassium ions during the cycling process, the Randles-Sevcik equation was utilized to calculate the ion diffusion rate of potassium ions[19]. Here, D_K represents the ion diffusion coefficient (cm^2/s), I_P denotes the peak current (A), n signifies the number of electrons transferred during the electrode reaction, A denotes the electrode area (cm^2), C_0 indicates the bulk concentration of the active material in the solution (mol/cm^2), and v stands for the scan rate (V/s). By calculating the D values at different scan rates, it can be observed that the diffusion coefficient of potassium ions in CuNi-KHP material is approximately 1.48974×10^{-11} cm^2/s, which is superior to that of other potassium-ion supercapacitor electrode materials ($3.4\times10-16$ cm^2/s),the supporting information Table 2 for details. A higher D value indicates rapid extraction/insertion of potassium ions in the electrode material. However, compared to MOF derivatives, there are still deficiencies due to the reduction of organic components in the derivatives, which results in better conductivity and is more conducive to ion migration.

Based on the Nicholson-Shain equation, the number of charge transfers during the reaction process is n=1, indicating that the pseudocapacitance process primarily involves the transfer of a single electron. Furthermore, the electrode equations ***(1)(2)*** are inferred based on two mechanisms***:***

$$\boldsymbol{Ep=E_0+\alpha n/FRT[0.78+\ln(D_{1/2}/k_0)+0.5\ln(\alpha nFv/RT)]} \quad \boldsymbol{XI}$$

$$\textbf{Ni (II) + OH}^- \leftrightarrow \textbf{Ni (II) (OH)aq+K}^+ \textbf{+ e}^- \leftrightarrow \textbf{Ni (III)(OH) aqK} \quad \textit{(1)}$$

$$\textbf{Cu(II)+OH}^- \textbf{+e}^- \textbf{+K}^+ \leftrightarrow \textbf{Cu(II)(OH)aqK} \quad \textit{(2)}$$

Next, the electrochemical performance of CuNi-KHP in hybrid potassium-ion

supercapacitors was tested.The power density (P) and energy density (E) of the energy storage devices were calculated based on the following equations:

$$E = \frac{1}{2} C \Delta V^2 \quad \textbf{XII}$$

$$P = \frac{E}{\Delta t} \quad \textbf{XIII}$$

References

[1] C. Chen, M.K. Wu, K. Tao, J.J. Zhou, Y.L. Li, X. Han, L.J.D.T. Han, Formation of bimetallic metal–organic framework nanosheets and their derived porous nickel–cobalt sulfides for supercapacitors, 47 (2018).

[2] L. Feng, K.Y. Wang, G.S. Day, H.C.J.C.S.r. Zhou, The chemistry of multi-component and hierarchical framework compounds, 48 (2019) 4823-4853.

[3] S. Mishra, M.K. Singh, D. Pandey, D.K. Rai, A. Raghuvanshi, A two-dimensional semiconducting Cu(i)-MOF for binder and conductive additive-free supercapattery, Journal of Materials Chemistry A, 12 (2024) 4534-4543.

[4] S. Gao, Y. Sui, F. Wei, J. Qi, Q. Meng, Y. He, Facile synthesis of cuboid Ni-MOF for high-performance supercapacitors, Journal of Materials Science, 53 (2018) 6807-6818.

[5] J. Khan, N. Shakeel, A. Arshad, M. Imran Saleem, A. Ali Al-Kahtani, Copper-based Para-Phthalic Acid Metal-Organic Framework: An efficient anodic material for super-capattery hybrid systems, Materials Chemistry and Physics, 326 (2024).

[6] J. Yang, C. Zheng, P. Xiong, Y. Li, M. Wei, Zn-doped Ni-MOF material with a high supercapacitive performance, J. Mater. Chem. A, 2 (2014) 19005-19010.

[7] Hai-Meng, Jing-Wei, Shuang, Chong, Jiang, Jun-Hua, Wei, Ya-Pan, Jun, Z.J.I. chemistry, Stable Bimetal-MOF Ultrathin Nanosheets for Pseudocapacitors with Enhanced Performance, 58 (2019) 9543-9547.

[8] I. Ntoukas, R. Lan, C. Milanese, M. Walker, S.W. Donne, A.J. Roberts, E.I. Gkanas, Ni/Co bimetallic flower-like metal–organic frameworks with enhanced performance for high-power energy storage applications, MRS Communications, 14 (2023) 69-75.

[9] N.H.N. Azman, M.M. Alias, Y. Sulaiman, HKUST-1 as a Positive Electrode Material for Supercapattery, Energies, 16 (2023) 7072.

[10] M. Ojha, B. Wu, M. Deepa, Cost-effective MIL-53 (Cr) metal–organic framework-based supercapacitors encompassing fast-ion (Li+/H+/Na+) conductors, ACS Applied Energy Materials, 4 (2021) 4729-4743.

[11] X. Li, R. Wang, Y. Yu, X. Wang, T. Gao, W. Lü, T. Yao, B. Song, MOF-derived Multi-Shelled NiP2 Microspheres as High-Performance Anode Materials for Sodium-/Potassium-Ion Batteries, Advanced Energy Sustainability Research, 3 (2022) 2200010.

[12] H. Zhou, G. Zhu, S. Dong, P. Liu, Y. Lu, Z. Zhou, S. Cao, Y. Zhang, H. Pang, Ethanol-induced Ni2+-intercalated cobalt organic frameworks on vanadium pentoxide for synergistically enhancing the performance of 3D-printed micro-supercapacitors, Advanced Materials, 35 (2023) 2211523.
[13] C. Yang, X. Li, L. Yu, X. Liu, J. Yang, M. Wei, A new promising Ni-MOF superstructure for high-performance supercapacitors, Chemical Communications, 56 (2020) 1803-1806.
[14] W. Zhao, T. Chen, W. Wang, B. Jin, J. Peng, S. Bi, M. Jiang, S. Liu, Q. Zhao, W. Huang, Conductive Ni3 (HITP) 2 MOFs thin films for flexible transparent supercapacitors with high rate capability, Science Bulletin, 65 (2020) 1803-1811.
[15] M. Sathiya, A.S. Prakash, K. Ramesha, J.M. Tarascon, A.K.J.J.o.t.A.C.S. Shukla, V2O5-anchored carbon nanotubes for enhanced electrochemical energy storage, 133 (2011) 16291.
[16] Advanced Energy Storage Devices: Basic Principles, Analytical Methods, and Rational Materials Design, Advanced ence, 5 (2018).
[17] V. Augustyn, J. Come, M.A. Lowe, J.W. Kim, P.L. Taberna, S.H. Tolbert, H.D. Abru?a, P. Simon, B.J.N.M. Dunn, High-rate electrochemical energy storage through Li+ intercalation pseudocapacitance, 12 (2013).
[18] J. Come, P.L. Taberna, S. Hamelet, C. Masquelier, P. Simon, Electrochemical Kinetic Study of LiFePO4 Using Cavity Microelectrode, Journal of The Electrochemical Society, 158 (2011).
[19] H.V. Ramasamy, B. Senthilkumar, P. Barpanda, Y.-S. Lee, Superior potassium-ion hybrid capacitor based on novel P3-type layered K0. 45Mn0. 5Co0. 5O2 as high capacity cathode, Chemical Engineering Journal, 368 (2019) 235-243.